LETTERS

Bistability of atmospheric oxygen and the Great Oxidation

Colin Goldblatt[1,2], Timothy M. Lenton[1] & Andrew J. Watson[1]

The history of the Earth has been characterized by a series of major transitions separated by long periods of relative stability[1]. The largest chemical transition was the 'Great Oxidation', approximately 2.4 billion years ago, when atmospheric oxygen concentrations rose from less than 10^{-5} of the present atmospheric level (PAL) to more than 0.01 PAL, and possibly[2] to more than 0.1 PAL. This transition took place long after oxygenic photosynthesis is thought to have evolved[3–5], but the causes of this delay and of the Great Oxidation itself remain uncertain[6–11]. Here we show that the origin of oxygenic photosynthesis gave rise to two simultaneously stable steady states for atmospheric oxygen. The existence of a low-oxygen (less than 10^{-5} PAL) steady state explains how a reducing atmosphere persisted for at least 300 million years after the onset of oxygenic photosynthesis. The Great Oxidation can be understood as a switch to the high-oxygen (more than 5×10^{-3} PAL) steady state. The bistability arises because ultraviolet shielding of the troposphere by ozone becomes effective once oxygen levels exceed 10^{-5} PAL, causing a nonlinear increase in the lifetime of atmospheric oxygen. Our results indicate that the existence of oxygenic photosynthesis is not a sufficient condition for either an oxygen-rich atmosphere or the presence of an ozone layer, which has implications for detecting life on other planets using atmospheric analysis[12,13] and for the evolution of multicellular life.

Before the origin of life, photochemical models[14] predict oxygen levels to have been $O_2 < 10^{-12}$ PAL. The recent discovery of mass independent fractionation (MIF) of sulphur isotopes[15] before 2.45 billion years ago (Gyr ago), constrains[16] O_2 to $<10^{-5}$ PAL. The MIF signal is absent in samples 2.33 Gyr old and younger[17], indicating that the Great Oxidation occurred approximately 2.4 Gyr ago. Geological and biological constraints indicate oxygen levels consistently >0.01 PAL after the Great Oxidation, and possibly >0.1 PAL. Compilations of MIF data and all geological constraints on palaeo-oxygen are included as Supplementary Information. The Great Oxidation would be most easily understood as the immediate consequence of the origin of oxygenic photosynthesis[18], but evidence from biomarkers[3–5] suggests this innovation had occurred at least 300 Myr earlier, by 2.7 Gyr ago. Recent hypotheses for the cause are: an increase in the oxidation state of mantle outgassing[6,8], but this appears to contradict geological constraints[9,19]; or a progressive oxidation of the crust, leading to a decreased flux of metamorphic reductants[10,11], but the mechanism of the required oxidation is unclear[9]. These hypotheses assume that the Great Oxidation was triggered when the oxygen source exceeded the input of volcanic and metamorphic reductants[6–9,11].

Our conceptual model of the global reduction–oxidation (redox) system (Fig. 1) explains the stability of oxygen levels each side of the Great Oxidation, the delay from the origin of oxygenic photosynthesis and the apperent rapidity and irreversibility of the transition. The rationale for the model is given here and it is described fully in the Methods and Supplementary Information.

Organisms play a pivotal role in the global redox system, generating fluxes of both oxidized and reduced gases to the atmosphere. Oxygenic photosynthesis is summarized thus:

$$CO_2 + H_2O + h\nu \rightarrow CH_2O + O_2 \quad (1)$$

where $h\nu$ indicates photosynthetically active radiation.

Today, around half of the carbon fixed is consumed internally by photosynthetic organisms in aerobic respiration, the reverse of equation (1). The remainder, the net primary productivity, is available to other organisms. The principal metabolic path for this carbon today is heterotrophic aerobic respiration, but this is inhibited below the Pasteur point, $O_2 \approx 0.01$ PAL. The metabolic pathway effective in anoxic conditions is fermentation followed by acetogenic methanogenesis:

$$2CH_2O \rightarrow CH_3COOH \rightarrow CH_4 + CO_2 \quad (2)$$

Oxygenic photosynthesis followed by fermentation and methanogenesis is summarized:

$$CO_2 + H_2O + h\nu \rightarrow \frac{1}{2}CH_4 + \frac{1}{2}CO_2 + O_2 \quad (3)$$

This is likely to have been the major metabolic path before the Great Oxidation. If there is sufficient ambient oxygen ($O_2 > 2 \times 10^{-4}$ PAL), methane-oxidizing bacteria (methanotrophs) will consume

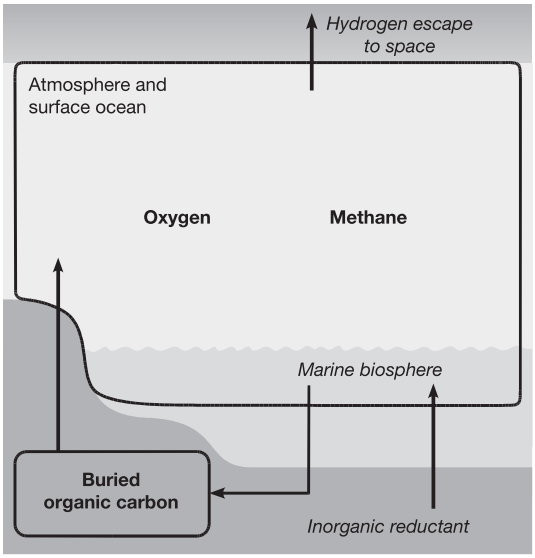

Figure 1 | Model schematic. We resolve methane and oxygen abundances in the atmosphere and surface ocean and a buried organic carbon in the crust.

[1]School of Environmental Sciences, University of East Anglia, Norwich, NR4 7TJ, UK. [2]Centre for Ecology and Hydrology, Edinburgh Research Station, Bush Estate, Penicuik, Midlothian, EH26 0QB, UK.

some of the methane and oxygen produced:

$$CH_4 + 2O_2 \rightarrow CO_2 + 2H_2O \quad (4)$$

but the remainder will be a flux of both methane and oxygen to the atmosphere in a 1:2 stoichiometric ratio. The fraction of the net primary productivity which has this fate, Ω_{O_2}, is higher in a low-oxygen atmosphere.

We describe the overall redox balance of the atmosphere–ocean system with a net input of reducing material represented by an input r of ferrous iron, burial and weathering of organic carbon and an oxidation due to loss of hydrogen to space sM, where s is a limiting flux constant[10] and M is the amount of methane in the atmosphere (see Supplementary Information).

Once oxygenic photosynthesis is well established with assumed net primary productivity N, the oxygen flux from the biosphere is $\Omega_{O_2}N$, representing the oxygen source from oxygenic photosynthesis, with the oxygen used in heterotrophic respiration and by methanotrophs subtracted. The corresponding methane flux is $\frac{1}{2}\Omega_{O_2}N$, from methanogenic decomposition of organic matter with consumption by methanotrophs subtracted. Thus the early Earth's biosphere, like today's, promoted an atmosphere in strong thermodynamic disequilibrium[12,13]. The dominant process in restoring equilibrium is atmospheric methane oxidation. This can be summarized with the stoichiometry of equation (4), but takes place as a series of reactions, some of which are photochemically mediated. We empirically parameterize this flux as a function of methane and oxygen abundances, fitting it to the results of detailed photochemical models[16,20,21] that resolve these reactions, obtaining oxidation rate $\Psi_{O_2}M^{0.7}$, where Ψ_{O_2} is a polynomial function of oxygen concentration (see Supplementary Information). An important property of the atmospheric chemistry embodied in Ψ_{O_2} is that, once oxygen has increased to a certain level, an ozone layer forms, shielding the troposphere from ultraviolet radiation. This dramatically decreases the rate of photolysis of water vapour in the troposphere, reducing hydroxyl radical availability, and thus suppressing the rate of methane oxidation[16,22].

Proxies indicate that either side of the Great Oxidation oxygen concentrations were relatively stable for 10^8–10^9 years, so these should correspond to steady-state solutions of our model. Steady-state methane balances net input r and output sM of reductant from the atmosphere–ocean system, giving:

$$M = \frac{r}{s} \quad (5)$$

The steady state for oxygen is dominated by the balance of production by the biosphere and loss of oxidizing methane; by substituting $M = r/s$ oxygen abundance is found as the solutions of:

$$\Omega_{O_2}N - \Psi_{O_2}\left(\frac{r}{s}\right)^{0.7} = 0 \quad (6)$$

There are two sets of stable steady-state solutions for oxygen in the presence of oxygenic photosynthesis (Fig. 2); high oxygen ($O_2 > 5 \times 10^{-3}$ PAL) and low oxygen ($O_2 < 10^{-5}$ PAL). Where these overlap, they are separated by an unstable steady-state solution. The cause of the bistability is a strong nonlinear positive feedback on oxygen levels. Once oxygen exceeds 2×10^{-5} PAL an ozone layer starts to form, decreasing the rate of methane oxidation. This reduced oxygen sink causes oxygen levels to increase, promoting the formation of the ozone layer. Oxygen continues to rise until the photochemical loss again balances the biospheric source. The level of the high-oxygen stable steady state is decreased by negative feedback within the biosphere; as oxygen increases, methanotrophy and heterotrophic respiration become effective at thresholds of 2×10^{-4} PAL and 0.01 PAL respectively, decreasing the fluxes of methane and oxygen to the atmosphere.

The low-oxygen solution is consistent with the MIF constraint of $O_2 < 10^{-5}$ PAL before the Great Oxidation. It is maintained in the presence of oxygenic photosynthesis, explaining the time lag between the origin of oxygenic photosynthesis and the Great Oxidation. The high-oxygen solution is consistent with proxy constraints following the Great Oxidation (Supplementary Fig. 1).

We hypothesize that the Great Oxidation corresponded to a switch between stable steady states when oxygen exceeded 10^{-5} PAL and an ozone layer developed. This contrasts with previous assumptions[6–9,11] that it occurred when the oxygen source from carbon burial exceeded the input of volcanic and metamorphic reductants. The system was probably in the bistable region shortly before the Great Oxidation (Fig. 2). Increasing N, or decreasing r, would mean that only the high-oxygen solution could exist, forcing the switch. A perturbation to the carbon cycle could also cause the transition, with the system remaining in the bistable region. Two plausible scenarios are outlined below.

Contemporaneous with the Great Oxidation, there is a marked decrease in banded iron formations (BIFs) in the sedimentary record approximately 2.4 Gyr ago (ref. 23), possibly caused by the cessation of a mantle superplume event[7]. Taking BIF deposition as a proxy of r implies a significant decrease in r (Fig. 2). With present productivity, the enhanced reductant input during BIF deposition[2] would correspond to oxygen in the bistable region ($O_2 \sim 10^{-6}$ PAL for the low-oxygen solution), whereas the present input of reduced iron to the ocean, with present productivity, corresponds to the monostable region of the high-oxygen solution ($O_2 \sim 10^{-1}$ PAL). Hence, decreasing r can trigger the Great Oxidation in our model (Fig. 3a). To maintain redox balance, the methane concentration of the atmosphere adjusts such that the loss of hydrogen to space balances the net input of reductant to the surface system. This adjustment takes around 50 million years during which there is a net oxidation as the

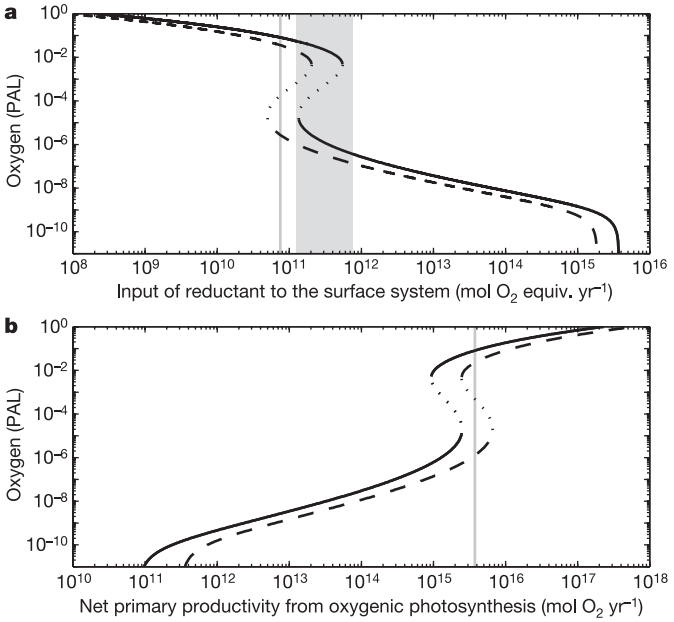

Figure 2 | Steady-state solutions for oxygen. Stable steady-state solutions are shown with solid and dashed lines, and unstable steady states with dotted lines. These are calculated with the full equation given in the Methods section; the simplified version given in the text is equivalent when oxygen exceeds 1×10^9 PAL. **a**, The solid line indicates modern marine net primary productivity ($N = 3.75 \times 10^{15}$ mol O_2 yr^{-1}) and the dashed line indicates half of the present N value for comparison. The shaded area shows constraints on iron deposition in BIFs before the Great Oxidation, which is taken as a proxy for reductant input. The minimum rate of iron deposition in the Hamersley BIF (2.69–2.44 Gyr ago; ref. 23) was 5×10^{11} mol Fe yr^{-1} and an upper bound for contemporaneous global deposition was 3×10^{12} mol Fe yr^{-1} (ref. 2), hence $1.25 \times 10^{11} < r < 7.5 \times 10^{11}$ mol O_2 equiv. yr^{-1}. The vertical grey line shows the present hydrothermal input of Fe to the ocean: 3×10^{11} mol Fe yr^{-1} (ref. 2), so $r = 7.5 \times 10^{10}$ mol O_2 equiv. yr^{-1}. **b**, The solid line indicates the present input of reduced iron to ocean, the dashed line indicates $r = 3 \times 10^{10}$ mol O_2 equiv. yr^{-1}, a possible value before the Great Oxidation. Modern marine N is shown as a vertical grey line.

system moves to its new steady state (Fig. 3b).

An alternative scenario is a small increase in N, and hence in organic carbon burial, with no change in r (Fig. 3c). As the size of the organic carbon reservoir adjusts, there is an oxygen source from excess organic carbon burial over weathering. Oxygen rises sufficiently to start ozone formation which causes the switch to high oxygen. Methane concentration, and hence oxidation from hydrogen escape, decreases transiently as the system adjusts. As a new steady state is achieved, organic carbon burial is balanced by weathering, atmospheric methane recovers and the net input of reductant is again balanced by hydrogen escape (Fig. 3d). The 3% increase in organic carbon burial assumed in this simulation would give a 0.23‰ increase in δ^{13}C carbonate (see Methods), which is less than the noise in that record[24]. Thus the Great Oxidation could have been triggered by a carbon cycle perturbation too small to be seen in the carbon isotope record.

There were probably fluctuations in the organic carbon cycle of this magnitude between the origin of oxygenic photosynthesis and the Great Oxidation. The low-oxygen solution in the bistable region resists perturbations poorly, so the transition to the high-oxygen solution would be likely. This suggests that the system was in the monostable low-oxygen region for most of this time and that the Great Oxidation was triggered by a decrease in reductant moving the system to the bistable region, followed by a small carbon cycle perturbation.

The bistability in oxygen describes a typical hysteresis loop (Fig. 2). If the Great Oxidation was triggered by a small decrease in r, causing a shift from the bistable lower branch to the monostable upper branch, a much larger increase in r would have been needed to switch the system back to the low-oxygen state. The transition from low to high oxygen (Fig. 3) would take 150,000 years if forced only by decreasing r, or 50,000 years with a carbon cycle perturbation, but the reverse would take 3–7 million years, owing to the larger reservoir of oxygen and smaller rate constant for methane oxidation, making high oxygen more resistant to perturbation. This may explain why oxygen never returned to Archean values after the Great Oxidation[2].

Our model suggests an earlier rise of oxygen from prebiotic levels of $\sim 10^{-12}$ PAL to the low-oxygen solution (Fig. 2). This occurred when the oxygen source from the biosphere, equal to N in anoxic conditions ($\Omega_{O_2} \rightarrow 1$), exceeded r. This probably occurred directly after the origin of oxygenic photosynthesis.

It has been argued that the Great Oxidation caused a large decline in atmospheric methane concentration, leading to extreme glaciation in the Palaeoproterozoic[25,26]. In transient runs of our model (see the right panels of Fig. 3), there is a rapid decrease in methane concentration by a factor of 2–6 while oxygen rises to the $>10^{-5}$ PAL threshold. The associated temperature drop is estimated to be 4–9 °C (see Supplementary Information). This may well have been sufficient to trigger extreme glaciation.

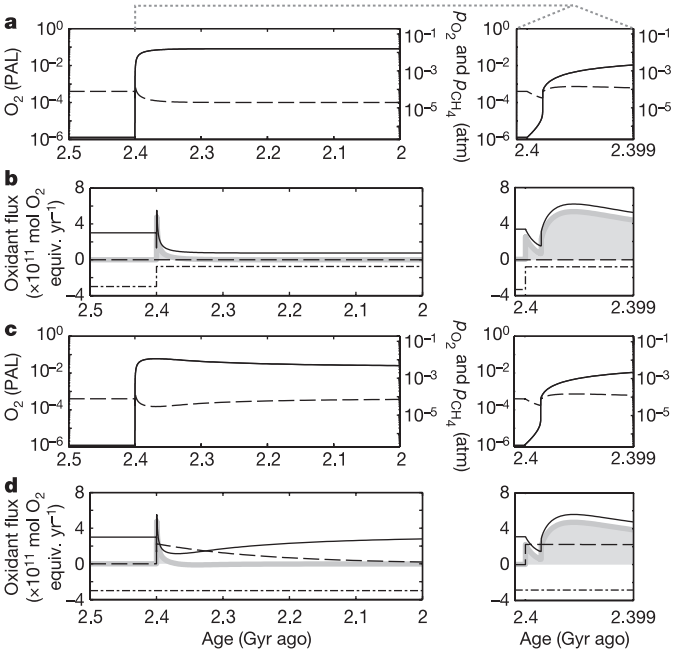

Figure 3 | Transient response to step changes at 2.4 Gyr ago representing possible triggers of the Great Oxidation. **a**, Response of oxygen (solid line, either scale) and methane (dashed line, right-hand scale) to a decrease in reductant input r from 3×10^{11} to 7.5×10^{10} mol O_2 equiv. yr^{-1}, inferred from decreased BIF deposition[2,23] with present $N = 3.75 \times 10^{15}$ mol $O_2\,yr^{-1}$. There is no significant change in the amount of buried organic carbon. **b**, Redox budget (boundary fluxes) of the surface system corresponding to **a**. Hydrogen escape is shown as a solid black line, the net change in the size of the organic carbon reservoir (burial minus weathering) as a dashed line and reductant input as a dot-dashed line. The grey line is the summation of these terms, the net oxidation rate of the surface system. The integral of this (shaded) is the total oxidation of the system, 3×10^{18} mol, which corresponds to the oxygen content of the atmosphere at the end of the model run. **c**, Response of oxygen and methane to a 3% increase in N from 3.6375×10^{15} to 3.75×10^{15} mol $O_2\,yr^{-1}$ with constant $r = 3 \times 10^{11}$ mol O_2 equiv. yr^{-1}. In response, the amount of buried organic carbon increases by 3% over ~500 million years after the Great Oxidation. As in **a**, the solid line indicates the oxygen response, and the dashed line the methane response. **d**, Redox budget of the surface system corresponding to **c**. The total oxidation is 9×10^{17} mol. The grey line and shading are as in **b**. The right panels expand the transitions shown in the left panels.

METHODS

Model structure. The model consists of a box representing the atmosphere and ocean mixed layer, in which the number of moles of O_2 (O) and CH_4 (M) are calculated, and a reservoir of organic carbon in the crust (C). Atmospheric gases are assumed to be dissolved in the mixed layer to saturation. The molar concentration of dissolved oxygen $[O] = (\alpha/\mu)O$ where $\mu = 1.773 \times 10^{20}$ mol is the number of moles in the present atmosphere and solubility is taken as $\alpha = 0.0013$ M.

Reductant input. The net input of inorganic reductant to the system is set as a boundary condition of r mol O_2 equiv. yr^{-1}, and is represented chemically by ferrous iron. It can include weathering of inorganic reductant in the crust and direct input from the mantle. The deep ocean is assumed to be anoxic, so any ferrous iron input here is taken to be transferred into the surface ocean. Anoxic photosynthesis in the surface ocean uses this ferrous iron as an electron donor:

$$4Fe^{2+} + CO_2 + 11H_2O + h\nu \rightarrow 4Fe(OH)_3 + CH_2O + 8H^+ \qquad (7)$$

and the resulting $Fe(OH)_3$ is precipitated as a BIF[27]. Hence reducing power is transferred to organic carbon.

Marine biosphere. Oxygenic photosynthesis is represented by an assumed net primary productivity of N mol $O_2\,yr^{-1}$, so the total organic carbon produced is $(N + r)$. The fraction of this consumed by heterotrophic respirers is $\gamma = O/(d_\gamma + O)$, where $d_\gamma = 1.36 \times 10^{19}$ mol, corresponding to the inhibition of aerobic respiration at the Pasteur point, $O_2 \approx 0.01$ PAL. The remaining organic matter is decomposed by fermenters and acetogenic methanogens. The fraction of the methane produced which is consumed by methanotrophs is $\delta = O/(d_\delta + O)$, where $d_\delta = 2.73 \times 10^{17}$ mol, equivalent to $[O] = 2\,\mu$M (ref. 28). Thus the fraction of the oxygen and methane produced that reaches the atmosphere is given $\Omega_{O_2} = (1 - \gamma)(1 - \delta)$.

Atmospheric chemistry. Fitting the methane oxidation rate to the results of detailed photochemical models, we obtain $\Psi M^{0.7}$, where M is the number of moles of CH_4, $\Psi = 10^{a_1\psi^4 + a_2\psi^3 + a_3\psi^2 + a_4\psi + a_5}$, $\psi = \log O$, $a_1 = 0.0030$, $a_2 = -0.1655$, $a_3 = 3.2305$, $a_4 = -25.8343$ and $a_5 = 71.5398$, valid for $10^8 < O < 10^{20}$ mol. This is derived in the Supplementary Information.

Hydrogen escape. Hydrogen escape to space is assumed to be diffusion limited, and so directly proportional to the total hydrogen mixing ratio in the upper atmosphere. With methane as the sole hydrogen-bearing species in our model, hydrogen loss is proportional to methane abundance, with rate sM where $s = 2.03 \times 10^{-5}\,yr^{-1}$ (ref. 10). Stoichiometrically, this is represented as[10]:

$$\begin{array}{c} CH_4 + h\nu \rightarrow 4H(\uparrow \text{space}) + C \\ C + O_2 \rightarrow CO_2 \\ \hline CH_4 + O_2 + h\nu \rightarrow 4H(\uparrow \text{space}) + CO_2 \end{array} \qquad (8)$$

This sink of methane and oxygen has a stoichiometric ratio of 1:1, but they are

produced in a ratio of 1:2, so hydrogen loss is a net source of oxidant. Water vapour is not a strong source of hydrogen for loss to space because little is able to pass the tropopause.

Crustal carbon cycle. Organic carbon burial is $\beta(N+r)$, a fraction of the organic carbon production. The rate of organic carbon weathering is wC, where the bulk weathering rate, $w = 6 \times 10^{-9}\,\mathrm{yr}^{-1}$, is set by analogy to present conditions and C is crustal organic carbon. At high oxygen levels, weathered material is oxidized directly. At low oxygen levels, oxidative weathering is ineffective and we assume that exposed organic carbon is consumed by organisms that transfer the reducing power to methane[29], which is subsequently oxidized in the atmosphere.

Model equations. The full algebraic derivation of our model is given in the Supplementary Information. The model equations are:

$$\frac{\mathrm{d}M}{\mathrm{d}t} = \frac{1}{2}\Omega_{\mathrm{O}_2}(N+r) - sM - \frac{1}{2}\Psi_{\mathrm{O}_2}M^{0.7} - \frac{1}{2}\Omega_{\mathrm{O}_2}(\beta(N+r) - wC) \quad (9)$$

$$\frac{\mathrm{d}O}{\mathrm{d}t} = \Omega_{\mathrm{O}_2}N - (1-\Omega_{\mathrm{O}_2})r - sM - \Psi_{\mathrm{O}_2}M^{0.7} + (1-\Omega_{\mathrm{O}_2})(\beta(N+r) - wC) \quad (10)$$

$$\frac{\mathrm{d}C}{\mathrm{d}t} = \beta(N+r) - wC \quad (11)$$

Steady-state solutions are found by setting equations (9)–(11) to zero. Rearranging gives $M = r/s$ and $C = \beta(N+r)/w$. Oxygen is found as the roots of $\Omega_{\mathrm{O}_2}N + (\Omega_{\mathrm{O}_2} - 2)r - \Psi_{\mathrm{O}_2}(r/s)^{0.7} = 0$. When $N \gg r$ these simplify to $C = \beta N/w$ and $\Omega_{\mathrm{O}_2}N - \Psi_{\mathrm{O}_2}(r/s)^{0.7} = 0$ (see Supplementary Information).

Carbon isotope calculations. The standard interpretation of the carbonate carbon isotope record is $f = (\delta_{\mathrm{carb}} - \delta_i)/(\delta_{\mathrm{carb}} - \delta_{\mathrm{org}})$ where f is the fraction of volcanic CO_2 buried as organic carbon and δ_{carb}, δ_i and δ_{org} are the $\delta^{13}C$ signals of carbonate carbon, volcanic CO_2 and organic carbon respectively. Typical values[30] are $\delta_{\mathrm{carb}} = 0‰$, $\delta_i = -6‰$ and $\delta_{\mathrm{org}} = -30‰$, giving $f = 0.2$. Our 3% increase in organic carbon burial (Fig. 3d) would correspond to $f = 0.206$ and hence $\delta_{\mathrm{carb}} = 0.23‰$.

Received 30 March; accepted 14 August 2006.

1. Lenton, T., Caldeira, K. & Szathmáry, E. in *Earth Systems Analysis Sustainability* (eds Schellnhuber, H., Crutzen, P., Clark, W., Claussen, M. & Held, H.) 29–52 (Dahlem Workshop Reports, Vol. 91, MIT Press, Cambridge, Massachusetts, 2004).
2. Holland, H. D. The oxygenation of the atmosphere and oceans. *Phil. Trans. Soc. B* **361,** 903–916 (2006).
3. Brocks, J. J., Logan, G. A., Buick, R. & Summons, R. Archean molecular fossils and the early rise of eukaryotes. *Science* **285,** 1033–1036 (1999).
4. Summons, R. E., Jahnke, L. L., Hope, J. M. & Logan, G. A. 2-Methylhopanoids as biomarkers for cyanobacterial oxygenic photosynthesis. *Nature* **400,** 554–557 (1999).
5. Brocks, J. J., Buick, R., Summons, R. E. & Logan, G. A. A reconstruction of Archean biological diversity based on molecular fossils from the 2.78 to 2.45 billion-year-old Mount Bruce Supergroup, Hamersley Basin, Western Australia. *Geochim. Cosmochim. Acta* **67,** 4321–4335 (2003).
6. Holland, H. D. Volcanic gases, black smokers, and the great oxidation event. *Geochim. Cosmochim. Acta* **66,** 3811–3826 (2002).
7. Barley, M. E., Bekker, A. & Krapež, B. Late Archean to early Paleoproterozoic global tectonics, environmental change and the rise of atmospheric oxygen. *Earth Planet. Sci. Lett.* **238,** 156–171 (2005).
8. Kump, L. R., Kasting, J. F. & Barley, M. E. Rise of atmospheric oxygen and the "upside-down" Archean mantle. *Geochem. Geophys. Geosyst.* **2**, doi:10.1029/2000GC000114 (2001).
9. Kasting, J. F. The rise of atmospheric oxygen. *Science* **293,** 819–820 (2001).
10. Catling, D., Zahnle, K. & McKay, C. Biogenic methane, hydrogen escape, and the irreversible oxidation of early Earth. *Science* **293,** 839–843 (2001).
11. Catling, D. C. & Claire, M. W. How Earth's atmosphere evolved to an oxic state: a status report. *Earth Planet. Sci. Lett.* **237,** 1–20 (2005).
12. Lovelock, J. A physical basis for life detection experiments. *Nature* **207,** 568–570 (1965).
13. Hitchcock, D. & Lovelock, J. Life detection by atmospheric analysis. *Icarus* **7,** 149–159 (1967).
14. Kasting, J. F., Liu, S. C. & Donahue, T. M. Oxygen levels in the prebiological atmosphere. *J. Geophys. Res.* **84,** 3097–3107 (1979).
15. Farquhar, J., Bao, H. & Thiemens, M. Atmospheric influence of Earth's earliest sulfur cycle. *Science* **289,** 757–758 (2000).
16. Pavlov, A. & Kasting, J. Mass-independent fractionation of sulfur isotopes in Archean sediments: strong evidence for an anoxic Archean atmosphere. *Astrobiology* **2,** 27–41 (2002).
17. Bekker, A. *et al.* Dating the rise of atmospheric oxygen. *Nature* **427,** 117–120 (2004).
18. Kopp, R. E., Kirschvink, J. L., Hilburn, I. A. & Nash, C. Z. The paleoproterozoic snowball Earth: A climate disaster triggered by the evolution of oxygenic photosynthesis. *Proc. Natl Acad. Sci. USA* **32,** 11131–11136 (2005).
19. Li, Z.-X. A. & Lee, C.-T. A. The constancy of upper mantle fO_2 through time inferred from V/Sc ratios in basalts. *Earth Planet. Sci. Lett.* **228,** 483–493 (2004).
20. Pavlov, A., Brown, L. & Kasting, J. UV shielding of NH_3 and O_2 by organic hazes in the Archean atmosphere. *J. Geophys. Res.* **106,** 23267–23287 (2001).
21. Pavlov, A., Hurtgen, M., Kasting, J. & Arthur, M. Methane-rich Proterozoic atmosphere? *Geology* **31,** 87–90 (2003).
22. Kasting, J. & Donahue, T. The evolution of the atmospheric ozone. *J. Geophys. Res.* **85,** 3255–3263 (1980).
23. Isley, A. E. & Abbott, D. H. Plume-related mafic volcanism and the deposition of banded iron formation. *J. Geophys. Res.* **104,** 15461–15477 (1999).
24. Shields, G. & Veizer, J. Precambrian marine carbonate isotope database: version 1.1. *Geochem. Geophys. Geosyst.* **3**, doi:10.1029/2001GC000266 (2002).
25. Pavlov, A. A., Kasting, J. F., Brown, L. L., Rages, K. A. & Freedman, R. Greenhouse warming by CH_4 in the atmosphere of early Earth. *J. Geophys. Res.* **105,** 11981–11990 (2000).
26. Kasting, J. F. Methane and climate during the precambrian era. *Precambrian Res.* **137,** 119–129 (2005).
27. Kharecha, P., Kasting, J. F. & Siefert, J. L. A coupled atmosphere-ecosystem model of the early Archean Earth. *Geobiology* **3,** 53–76 (2005).
28. Ren, T., Amaral, J. A. & Knowles, R. The response of methane consumption by pure cultures of methanotropic bacteria to oxygen. *Can. J. Microbiol.* **43,** 925–928 (1997).
29. Holland, H. D. Discussion of the article by A. C. Lasaga and H. Ohmoto on "The oxygen geochemical cycle: dynamics and stability", Geochim. Cosmochim. Acta 66, 361–381, 2002. *Geochim. Cosmochim. Acta* **67,** 787–789 (2003).
30. Hayes, J. M. & Waldbauer, J. R. The carbon cycle and associated redox processed through time. *Phil. Trans. R. Soc. B* **361,** 931–950 (2006).

Supplementary Information is linked to the online version of the paper at www.nature.com/nature.

Acknowledgements C.G. is funded by the Natural Environment Research Council. T.M.L. is supported by a Leverhulme Prize. We thank J. Kasting and L. Kump for comments on the manuscript. C.G. thanks J. Meiss for teaching dynamical systems.

Author Contributions T.M.L. and A.J.W suggested the study. C.G. wrote and analysed the model with supervision from T.M.L. and A.J.W., and led writing the paper.

Author Information Reprints and permissions information is available at www.nature.com/reprints. The authors declare that they have no competing financial interests. Correspondence and requests for materials should be addressed to C.G. (c.goldblatt@uea.ac.uk).